LC-HRMS-based phytochemical profiling of the ethanolic extract of Moringa oleifera seeds against toxic hepatotoxicity supported by in silico network design, molecular docking and simulation studies

Neha Gupta
Banaras Hindu University
Raghunath More
raghunath.more@bhu.ac.in

Banaras Hindu University
Jasmeet Singh
Banaras Hindu University
Bishnu Prasad Parida
Banaras Hindu University
Aabidha Anand
Banaras Hindu University
Atul Tiwari
Banaras Hindu University

Research Article

Keywords: Hepatoprotection, Toxic hepatitis, Moringa oleifera, LC-HRMS, Network pharmacology, MD simulation

Posted Date: April 16th, 2026

DOI: https://doi.org/10.21203/rs.3.rs-8794547/v1

Additional Declarations: No competing interests reported.

Abstract

Toxic hepatitis or drug-induced liver injury (DILI) has emerged as an escalating health concern over the past few years and is driven by the hepatic metabolism of xenobiotic compounds. The present study evaluated the hepatoprotective efficacy of Moringa oleifera seed extract (MOSE) using an integrated strategy that encompassed HRMS-based profiling, ADMET screening, Metascape-based network pharmacology, molecular docking via SMINA, and molecular dynamics (MD) simulations performed through GROMACS. LC-HRMS profiling identified 3,085 putative metabolites, of which 14 were selected based on their relative abundance. Rigorous ADMET screening resulted in three shortlisted compounds, namely, trans-3-indoleacrylic acid, (R)-prunasin, and 5-(4-morpholinyl)pyrazolo[1,5-a]quinazoline-3-carbonitrile, which were investigated in detail. Network pharmacology analysis revealed five topological hub genes, HRAS, PIK3CA, MMP9, LGALS3, and NFE2L2, as core regulators of extract-mediated protection against DILI. The identified targets from the similarity ensemble approach (SEA) were significantly enriched in essential biological pathways, including the apoptosis and chemical carcinogenesis-ROS pathways as revealed by Metascape. Molecular docking analysis with SMINA indicated strong binding efficacy, especially for (R)-prunasin toward HRAS (-9.20 kcal/mol). A 100 ns GROMACS MD simulation corroborated the robustness of the interaction stability under physiological conditions. These results suggest that Moringa oleifera seeds confer hepatoprotective effects through the coordinated modulation of multiple targets that support cell survival networks, activate antioxidants, and inhibit apoptosis. This study offers a molecular-level rationale for advancing standardized MOSE-based therapies for liver injury via integrative systems pharmacology approaches.

1. Introduction

Toxic hepatitis, commonly known as liver toxicity or drug-induced liver injury (DILI), is a major concern worldwide, with increasing incidence rates ranging from 12 persons per 100,000 individuals per year in South Korea(1) to an extrapolated frequency of 23.80 cases per 100,000 individuals among local Chinese inhabitants(2). Research indicates that exposure to toxic doses of certain substances, such as drugs, alcohol, and food supplements, can cause toxic hepatitis. In India, the leading causes of drug toxicity are anti-TB and anti-epileptic drugs(1). The heightened hepatic susceptibility to undesirable drug action is likely associated with its fundamental role in xenobiotic metabolism, followed by absorption through the gastrointestinal (GI) tract(3). Toxic hepatitis may develop acutely or chronically, depending on the nature and duration of exposure to drugs (intrinsic type), or may be determined by the interoperability of unpredictable environmental and host factors (idiosyncratic type)(4). Clinical features may range from asymptomatic enzyme elevation to life-threatening liver failure or cirrhosis. The pathophysiology of toxic hepatitis typically begins with the absorption of hepatotoxic agents through ingestion, inhalation, or dermal exposure. Once inside the body, these agents undergo biotransformation in the liver, primarily via cytochrome P450 enzymes(5). During this process, toxic metabolites can form that may cause direct hepatocellular damage, induce oxidative stress, deplete glutathione reserves, or trigger immune-mediated responses. The resulting hepatocellular injury can lead to necrosis, apoptosis, cholestasis, or fibrosis, depending on the extent and nature of the damage(6).

Medicinal plants have gained enormous importance over the years because of their ability to cure human health and combat various diseases. The therapeutic activity of medicinal plants is attributed to the wide array of phytochemicals present in them. These phytochemicals work to modulate multiple targets to alleviate several acute and chronic complications; hence, accurately determining the exact mechanism is still a task (7)(8). One such medicinal plant, Moringa oleifera Lam (family Moringaceae), also known as Kelor, Mlonge, Horseradish tree, Drumstick tree, Marango, Benzolive, Malunggay, Sajna and Sahijan, is highly cultivated in various regions around the world. It has been shown to have remarkable prophylactic and therapeutic properties, such as anti-microbial, anti-pyretic, anti-asthmatic, anthelminthic, hepatoprotective and anti-oxidant properties, in various studies and hence is also considered a “miracle tree”(9, 10). The versatility of Moringa oleifera extends beyond its medicinal properties, as it is also regarded for its edible seeds, flowers and leaves, which are ample in essential nutrients such as vitamins, minerals, and proteins. In addition, it is an excellent fertilizer and has a wide variety of uses in sustainable agricultural practices(11). In traditional medicinal practices, Moringa oleifera has been utilized for the treatment of hepatic ailments, inflammation-related disorders and metabolic dysfunctions, providing ethnopharmacological relevance for

the present study. Understanding the phytochemical constituents of moringa oleifera through more accurate and comprehensive techniques, such as HRMS, could lead to the development of new treatment methodologies for oxidative stress and inflammation-related diseases (12)(13).

To explore the metabolic diversity in a plant matrix, several chromatographic and spectrometric techniques, such as LC–MS, GC–MS, LC-ESI-MS, FT-IR, NMR, and HILIC, are employed, which facilitate qualitative and quantitative phytochemical assessment on the basis of their individual operational principles(14)(15)(16). Newer approaches, such as hybrid quadrupole-Orbitrap HRMS (Q-Orbitrap HRMS), have the additional benefit of enabling high-resolution and precise trace-level compound detection at low µg/kg concentrations(17).

The multi-mechanistic associations of these compounds with genes related to targeted and untargeted diseases led to the formation of a network. Network pharmacology, a computational technique, enables such a network to reveal drug-gene-disease interactions of medicinal plants through various platforms in a high-throughput manner. The mechanism of action of medicinal plants is elucidated by integrating metabolomics with this network pharmacology, which elucidates synergistic molecular combinations engaging with discrete targets within a network (18). Since most of the literature is emphasized on leaf-based interventions, the present study focused on the wide range of metabolites present in moringa oleifera seed extracts and their role in the treatment of various acute and chronic diseases, especially toxic hepatitis, through a network-based assessment of their multitarget therapeutic mechanisms. Molecular docking analyses were carried out to investigate the binding interaction patterns of key phytochemicals with hub targets associated with toxic hepatitis. The stability of the docked complexes under relevant physiological conditions was further validated via molecular dynamics simulations.

2. Materials and methods

2.1 Moringa oleifera seed collection and ethanolic extract preparation

The de-husked Moringa oleifera seeds were purchased from a local vendor of Varanasi and authenticated (No. DG/25–26/946) by the Department of Dravyaguna, Institute of Medical Sciences, Banaras Hindu University, Varanasi, India. The seeds were washed two to three times under running water and dried properly in the dark at room temperature. After that, the seeds were crushed by a mechanical grinder until a fine powder was obtained. A 50 g powdered seed sample was extracted in 175 mL of ethanol and 175 mL of distilled water (50:50) to prepare an ethanolic extract of moringa oleifera seeds. After 2–3 cycles, the extract was collected and then filtered with Whatman filter paper. The extract was dried and evaporated via a rotary evaporator at a controlled temperature of 45°C.

2.2 HRMS/MS profiling of Moringa oleifera seed extract

Phytochemical analysis of the dried MOSE extract was performed with a high-resolution mass spectrometry instrument (Dionex UltiMate 3000 RS Ultra high-performance liquid chromatography (UHPLC) for small molecule detection available at Central Discovery Centre (CDC), Banaras Hindu University. The HPLC column was made of Hypersil GOLD™ C18 Selectivity, with a diameter of 2.1 mm and a length of 100 mm, which allows entry of particles up to a size of 1.9 mm. Before the sample was injected into the UHPLC-HRMS system for phytochemical analysis, the dried MOSE extract (1 mg/ml) was first dissolved in a pure methanol solution and filtered. The total run time of the sample was 30 minutes, and the phytoconstituents were identified on the basis of their m/z ratios and retention times.

2.3 Selection and screening of target bioactive compounds

A total of 3086 bioactive compounds were obtained through HRMS analysis. The compounds with a percentage area max greater than 1 were taken for further analysis to prioritize abundant bioactive compounds. A total of fourteen compounds were chosen (Table 1). For ADMET analysis, these compounds were subjected to additional screening via the Swiss ADME (https://www.swissadme.ch/)(19), Protox 3.0 web server (https://tox.charite.de/protox3/)(20), and pkCSM databases (https://biosig.lab.uq.edu.au/pkcsm/)(21). ADMET (absorption, distribution, metabolism, excretion and toxicity) analysis estimates the potential toxicity of a drug in the system and the pathways with which it is absorbed, distributed, metabolized,

and eliminated in the body by employing graph-based signatures, machine learning algorithms and convolutional neural networks (CNNs). Understanding these characteristics is crucial for ensuring the safety and efficacy of pharmaceuticals. Key physicochemical descriptors, such as hydrogen bonding parameters (HBA, HBD), molar refractivity (MR), molecular weight (MW), topological polar surface area (TPSA), logarithmic lipophilicity (LogP) and drug likeness (DL), were predicted via SwissADME (Table 2B). Pharmacokinetic properties such as human intestinal absorption of the compound (HIA), Caco2 permeability, water solubility, absence of AMES toxicity, hERG inhibition, hepatotoxicity, pains alert, brenk alerts (< 1) and major CYP (CYP3A4 or CYP2D6) inhibition were considered through the pkCSM server (Table 2A). BBB permeation was not considered a stringent rejection criterion, as the therapeutic focus was on hepatic indications rather than CNS toxicity, although compounds with predicted neurotoxic effects were excluded. The Protox III database was used for the prediction of organ toxicity, toxicity endpoints, Tox 21 stress response pathways, Tox 21 nuclear receptor signaling pathways, molecular initiating events and metabolism. The compounds of the predicted toxicity classes I-III were eliminated. After rigorous screening, three compounds were finalized for further analysis: trans-3-indoleacrylic acid, (R)-prunasin and 5-(4-morpholinyl)pyrazolo[1,5-a]quinazoline-3-carbonitrile.

2.4 Identification of compounds and toxic hepatitis targets

Potential protein targets of each compound were predicted via the similarity ensemble approach (SEA) (https://sea.bkslab.org/)(22), which predicts statistically significant ligand-target interactions on the basis of chemical similarity to known bioactive compounds. The predictions were restricted to human protein targets with p values ≤ 1×10^{-8} and maximum Tanimoto coefficient (Max Tc) values ≥ 0.3 to ensure high confidence. The GeneCards (https://www.genecards.org/)(23) and DisGeNet version 25.4 (https://disgenet.com/)(24) databases were employed to retrieve toxic hepatitis-associated genes. Both gene lists were merged via their UniProt identifiers, and duplicate entries were removed, resulting in a nonredundant disease-related gene set.

2.5 Extraction of disease-relevant targets for individual compounds

The SEA targets of each compound were intersected with each other first and subsequently overlapped with toxic hepatitis targets with the help of Venny 2.1.0 (https://bioinfogp.cnb.csic.es/tools/venny/)(25) to ensure disease relevance while maintaining compound-level specificity, and to enable comparative assessment of overlapping or complementary mechanisms of action. The retrieved disease-associated targets were then integrated and deduplicated to generate a set of final extract-level nonoverlapping target proteins.

2.5 Protein–protein interaction network and hub gene screening

The protein–protein interaction (PPI) network was visualized via the STRING 12.0 server (https://string-db.org/)(26) using *Homo sapiens* as the experimental model at an optimum interaction score of 0.4 (medium confidence). This network was aligned via the CytoNCA application through Cytoscape version 3.10.4 (https://cytoscape.org/)(27) on the basis of three parameters, namely, degree, betweenness and closeness of the target genes, with no weight parameters.

2.6 Estimation of gene ontology and KEGG enrichment

To scrutinize gene ontology, the hub genes were entered into Metascape version v3.5.20250701 (https://metascape.org/gp/index.html#/main/step1)(28), with the input species set to *Homo sapiens* and the entire human genome used as the background reference for functional enrichment analysis. Metascape integrates annotations from multiple curated databases, including KEGG, Reactome, GO Biological Processes, and WikiPathways. Pathways with a threshold -log10 (FDR) value ≥-1.50 and a minimum gene count ≥ 3 were considered statistically significant. Non-hepatic pathways were manually ruled out to ensure their biological relevance to toxic hepatitis. The filtered outcomes were exported to R to generate a dot plot of fold enrichment mapped on the x-axis and relevant biological pathways on the y-axis, and a compound-target-pathway network was constructed via Cytoscape.

2.7 Molecular docking

The structural coordinates of the proteins corresponding to the hub genes HRAS, PIK3CA, MMP9, LGALS3 and NFE2L2 were sourced from the Protein Data Bank (https://www.rcsb.org/)(29) database, which has PDB IDs 9IAY, 8EXL, 6ESM, 6QLR, and

8XGK, respectively, on the basis of resolution, completeness of the protein structure, absence of mutations, etc. Each structure was cleaned by eliminating crystallographic water molecules, cofactors, ions and nonessential heteroatoms prior to docking, and proper protonation was ensured by adding missing hydrogen atoms and adjusting the pH. The prepared receptor files were independently docked with three bioactive ligands- trans-3-indoleacrylic acid, R-prunasin, and 5-(4-morpholinyl)pyrazolo[1,5-a]quinazoline-3-carbonitrile- using SMINA version 2020.12.10(30), an optimized implementation of AutoDock Vina 1.1.2, which retains a well-validated Vina scoring function and offers more efficient ligand-receptor conformational sampling. The grid box generation was defined via the autobox strategy, where its dimensions are derived from the coordinates of the co-crystallized native ligand present in each receptor protein to ensure relevant binding sites. Docking robustness and reliability were assessed by docking each compound-target pair independently at three exhaustiveness levels (8, 16 and 32).

2.8 Simulation

2.8.1 Simulation setup

R-Prunasin has emerged as the most promising ligand on the basis of its robust interactions and commendable docking score against HRAS. The structural stability and dynamic behavior of the (R)-Prunasin-HRAS complex under physiological conditions were assessed via molecular dynamics simulations, GROMACS version v.2025.3 (31), over 100 ns. Protein topology files were generated via the AMBER99SB-ILDN force field, whereas ligand parameters were obtained via ACPTYPE, which is based on GAFF, to ensure compatibility with the AMBER force fields. The complex was solvated in a triclinic simulation box containing explicit TIP3P water molecules, maintaining a minimum boundary of 1 nm between the box edge and proteins. The system was neutralized, and physiological ionic conditions were achieved by adding counterions.

2.8.2 Energy minimization and equilibration

Energy minimization of the system was performed via the steepest descent algorithm to eliminate steric clashes, followed by equilibration under a constant number of particles, volume and temperature (NVT ensemble) at 300 K via a velocity-rescaling thermostat and a constant number of particles, pressure, and temperature (NPT ensemble) at 1 bar via a Parrinello–Rahman barostat. Position restraints were applied to maintain the stability of the complex.

2.8.3 Production MD simulation and trajectory analysis

Unrestrained 100 ns MD simulations were performed via a 2fs time step. Electrostatic interactions were treated with the particle–mesh Ewald (PME) method, whereas Coulomb and van der Waals interactions were calculated via the Verlet cutoff scheme with a 1.0 nm cutoff radius(32, 33). Trajectory analysis was performed via the standard GROMACS tool. Convergence parameters of the protein backbone and ligand, residue flexibility analysis, structural compactness and interaction energy plots were studied.

3. Results

3.1 Identification of the Phyto-constituents of ethanolic extracts of moringa oleifera through HRMS analysis

HR-MS analysis of the MOSE extract revealed a chemically diverse spectrum of 3085 compounds in positive and negative ion modes, supporting its association with antioxidant, anti-inflammatory and hepatoprotective effects. Fourteen metabolites were shortlisted for further investigation on the basis of their relative abundance, exhibiting a peak area maximum percentage greater than 1. Key properties such as their structure, chemical formula, retention time, M/Z ratio, peak area percentage and mode of analysis are listed in Table 1.

3.2 ADMET screening of compounds present in MOSE extracts

The pharmacokinetic and physicochemical properties of all fourteen selected compounds are shown in Tables 2(A) and 2(B). Compounds violating critical ADMET criteria, including Lipinski/Veber rules, PAINS warnings, major CYP inhibition (CYP3A4,

CYP2D6), hepatotoxic predictions or low LD_{50}/LOAEL safety, were systematically filtered out. The rigorous screening process revealed three compounds with safe toxicity profiles and high oral absorption: trans-3-indoleacrylic acid, (R)-prunasin and 5-(4-morpholinyl)pyrazolo[1,5-a]quinazoline-3-carbonitrile. These compounds were selected for subsequent docking and molecular dynamics investigations (Supplementary Table S1).

Table 2
(A): Pharmacokinetic properties of the compounds present in the ethanolic extract of Moringa oleifera.

Name of compound	GI Absorption	BBB permeation	Water solubility	CaCo2 permeability	CYP2D6 inhibition	CYP3A4 inhibition
trans-3-Indoleacrylic acid	High	Yes	High	High	No	No
(R)-Prunasin	High	No	High	Moderate	No	No
4-(Methoxymethyl)-6-methyl-5-nitro-2-[(3,4,5-trimethoxybenzyl)amino]nicotinonitrile	High	No	Moderate	Moderate	No	Yes
1-{4-[3-(2-Methyl-2-propanyl)-1,2,4-oxadiazol-5-yl]-2-pyridinyl}-1H-imidazole-4-carboxylic acid	High	No	Moderate	High	No	No
(2E)-3-{3-[(2-Hydroxyethyl)(methyl)sulfamoyl]-4,5-dimethoxyphenyl}acrylic acid	High	No	High	Moderate	No	No
Pestalotiopyrone L	High	No	High	Moderate	No	No
1-phenylpropane-1_2-dione	High	Yes	High	High	No	No
pyridoxal isonicotinoyl hydrazone	High	No	High	Moderate	No	No
(S)-4-Hydroxymandelonitrile	High	No	High	Moderate	No	Yes
Adenosine	Low	No	High	Moderate	No	No
4-methylthiobutanaldoxime	High	Yes	High	High	No	No
(9S_10S)-9_10-Dihydroxyoctadecanoate	High	No	Low	Moderate	Yes	No
5-(4-Morpholinyl)pyrazolo[1,5-a]quinazoline-3-carbonitrile	High	Yes	High	High	No	No
5-[4-(Allyloxy)-3-methoxyphenyl]-2-amino-5,8-dihydropyrido[2,3-d]pyrimidine-4,7(1H,6H)-dione	High	No	High	Low	No	No

Table 2
(B): Physico-chemical properties of the compounds present in MOSE extract.

Name of compound	HBA	HBD	MLOGP	MR	TPSA (Å²)	Lipnski-Veber compliance
trans-3-Indoleacrylic acid	2	2	1.32	52.55	53.09	Yes
(R)-Prunasin	7	4	-1.58	69.51	132	Yes
4-(Methoxymethyl)-6-methyl-5-nitro-2-[(3,4,5-trimethoxybenzyl)amino]nicotinonitrile	8	1	-0.39	106.87	131.45	Yes
1-{4-[3-(2-Methyl-2-propanyl)-1,2,4-oxadiazol-5-yl]-2-pyridinyl}-1H-imidazole-4-carboxylic acid	7	1	1.14	80.88	106.93	Yes
(2E)-3-{3-[(2-Hydroxyethyl)(methyl)sulfamoyl]-4,5-dimethoxyphenyl}acrylic acid	8	2	-0.2	82.86	121.75	Yes
Pestalotiopyrone L	7	2	0.08	78.38	106.20	Yes
1-phenylpropane-1_2-dione	4	0	1.36	83.29	62.28	Yes
pyridoxal isonicotinoyl hydrazone	6	3	-0.56	76.32	107.70	Yes
(S)-4-Hydroxymandelonitrile	3	2	0.24	39.15	64.25	Yes
Adenosine	7	4	-2.72	62.67	139.54	Yes
4-methylthiobutanaldoxime	2	1	0.89	38.15	57.89	Yes
(9S_10S)-9_10-Dihydroxyoctadecanoate	4	2	2.94	90.79	80.59	No (Veber)
5-(4-Morpholinyl)pyrazolo[1,5-a]quinazoline-3-carbonitrile	4	0	1.4	80.94	66.45	Yes
5-[4-(Allyloxy)-3-methoxyphenyl]-2-amino-5,8-dihydropyrido[2,3-d]pyrimidine-4,7(1H,6H)-dione	5	3	0.68	95.97	119.33	Yes

3.3 SEA-based target prediction

There are 30 SEA-predicted human targets for trans-3-indoleacrylic acid, 28 targets for (R)-prunasin and 23 targets for 5-(4-morpholinyl)pyrazolo[1,5-a]quinazoline-3-carbonitrile. The compound-specific SEA targets independently overlapped with the toxic hepatitis targets retrieved from DisGeNET (301 targets) and GeneCards (328 targets). Out of the 629 genes associated with toxic hepatitis, 588 genes were retained after duplication. The trans-3-indoleacrylic acid targets presented the highest target count (8 targets), followed by (R)-prunasin (3 targets) and 5-(4-morpholinyl)pyrazolo[1,5-a]quinazoline-3-carbonitrile (2 targets). The interaction of these target sets with each other suggested limited overlap, indicating that the multiple components of the extract contribute through different pathways against toxic hepatitis. Subsequent integration of these disease-relevant targets resulted in a final extract-level target set comprising a total of 13 unique targets.

3.4 Protein–protein interaction (PPI) network construction and identification of hub genes

An interaction network of these 13 genes was built from the STRING webserver (Fig. 2A). These genes were exported to Cytoscape (3.10.4), and the top five hub genes (MMP9, NFE2L2, HRAS, PIK3CA, and LGALS3) were selected through CytoNCA application from Cytoscape (Fig. 2B) on the basis of their degree, betweenness centrality and proximity without weight parameters; strong evidence links; and direct roles in pathways involved in drug-induced liver toxicity (DILI) or toxic hepatitis. These hub genes were ranked by cytoHubba through the MCC algorithm (Fig. 2C).

3.5 Pathway enrichment of the hub genes associated with toxic hepatitis

The pathway enrichment of these hub genes through Metascape revealed significant involvement of 9 major pathways contributing to toxic hepatitis. Each pathway is mediated by a combination of 3 genes (Fig. 3). The most prominently enriched pathway was related to chemical carcinogenesis- reactive oxygen species. This highlights oxidative stress as the main cause of toxic hepatitis and the combined roles of HRAS, NFE2L2, and PIK3CA in modulating oxidative stress-induced cellular signaling. Pathways related to apoptosis, such as the regulation and negative regulation of apoptotic signaling, are mediated by LGALS3, MMP9 and NFE2L2 and significantly contribute to programmed cell death due to the loss of hepatocytes in toxic hepatitis. HRAS, MMP9 and PIK3CA are involved in signaling via receptor tyrosine kinases and cell surface receptor protein tyrosine kinase signaling pathways that depend on growth factors and stress-activated cascades. In addition, they make relevant contributions to pathways related to the cellular response to abiotic and environmental stimuli. The key hub genes involved in nuclear receptor signaling pathways were HRAS, MMP9 and PIK3CA, and those involved in the response to peptide hormones were HRAS, NFE2L2 and PIK3CA. The interactions among these compounds, genes and enriched biological pathways are shown in Fig. 4.

3.6 Molecular Docking Analysis of Hub Genes with Compounds via SMINA

Molecular docking of the compounds trans-3-indoleacrylic acid, R-prunasin, and 5-(4-morpholinyl)pyrazolo[1,5-a]quinazoline-3-carbonitrile against five hub targets (MMP9, LGALS3, HRAS, PIK3CA and NFE2L2) at exhaustiveness values of 8, 16 and 32 indicated consistent and reliable binding affinities across repeated runs, with slight variations (Table 3).

Trans-3-indoleacrylic acid had the highest binding affinity for HRAS (-7.70 ± 0.00 kcal/mol) > PIK3CA (-7.50 ± 0.00 kcal/mol) and NFE2L2 (-6.03 ± 0.06 kcal/mol), followed by LGALS3 (-5.60 ± 0.00 kcal/mol) and MMP9 (-5.43 ± 0.06 kcal/mol). R-Prunasin showed excellent binding affinities with HRAS (-9.20 ± 0.00 kcal/mol) > PIK3CA (-7.90 ± 0.00 kcal/mol) > LGALS3 (-7.00 ± 0.00 kcal/mol) > NFE2L2 (-6.97 ± 0.06) > MMP9 (-6.40 ± 0.00 kcal/mol), whereas 5-(4-morpholinyl)pyrazolo[1,5-a]quinazoline-3-carbonitrile had maximum affinity with PIK3CA (-7.77 ± 0.06 kcal/mol) > HRAS (-7.70 ± 0.00) > LGALS3 (-6.63 ± 0.06 kcal/mol) > NFE2L2 (-6.60 ± 0.00 kcal/mol) > MMP9 (-5.70 ± 0.00 kcal/mol). The results demonstrated exceptionally high binding affinity between R-Prunasin and HRAS, suggesting hydrophobic interactions in the direct active sites. Conversely, the interactions of PIK3CA, LGALS3, NFE2L2 and MMP9 with all three compounds presented moderate docking scores, suggesting that modulatory interactions occur instead of direct active site targeting. The Biovia Discovery visualization tool was used to visualize these compound–target interactions. The 2D and 3D images of the top 3 docked complexes, R-Prunasin with HRAS, R-Prunasin with PIK3CA and 5-(4-morpholinyl)pyrazolo[1,5-a]quinazoline-3-carbonitrile with PIK3CA, are shown in Fig. 5.

Table 3
Docking scores (kcal/mol) of each compound–gene pair in three consecutive runs obtained via SMINA at exhaustiveness levels of 8, 16 and 32. Cpd_1 = trans-3-indoleacrylic acid; Cpd_2 = R-prunasin; Cpd_3 = 5-(4-morpholinyl)pyrazolo[1,5-a]quinazoline-3-carbonitrile.

Compound	Hub gene (PDB ID)	Run 1 (E:8)	Run2 (E:16)	Run 3 (E:32)	Mean ± SD
Cpd_1	HRAS (9IAY)	-7.70	-7.70	-7.70	-7.70 ± 0.00
	PIK3CA (8EXL)	-7.50	-7.50	-7.50	-7.50 ± 0.00
	MMP9 (6ESM)	-5.40	-5.50	-5.40	-5.43 ± 0.06
	LGALS3 (6QLR)	-5.60	-5.60	-5.60	-5.60 ± 0.00
	NFE2L2 (8XGX)	-6.00	-6.00	-6.10	-6.03 ± 0.06
Cpd_2	HRAS (9IAY)	-9.20	-9.20	-9.20	-9.20 ± 0.00
	PIK3CA (8EXL)	-7.90	-7.90	-7.90	-7.90 ± 0.00
	MMP9 (6ESM)	-6.40	-6.40	-6.40	-6.40 ± 0.00
	LGALS3 (6QLR)	-7.00	-7.00	-7.00	-7.00 ± 0.00
	NFE2L2 (8XGX)	-6.90	-7.00	-7.00	-6.97 ± 0.06
Cpd_3	HRAS (9IAY)	-7.70	-7.70	-7.70	-7.70 ± 0.00
	PIK3CA (8EXL)	-7.70	-7.80	-7.80	-7.77 ± 0.06
	MMP9 (6ESM	-5.70	-5.70	-5.70	-5.70 ± 0.00
	LGALS3 (6QLR)	-6.60	-6.60	-6.70	-6.63 ± 0.06
	NFE2L2 (8XGX)	-6.60	-6.60	-6.60	-6.60 ± 0.00

3.7 Simulation

The protein backbone RMSD for the 100 ns molecular dynamics simulation (Fig. 6A) showed rapid convergence at approximately 0.12–0.27 nm, suggesting early attainment of an energetically favorable state of the system. Ligand RMSD (Fig. 6B) indicated the continuous association of (R)-prunasin with HRAS across the simulation timeframe. Although moderate fluctuations were evident during the mid-trajectory, the ligand remained consistently bound. A residue flexibility analysis (RMSF) plot (Fig. 6C) demonstrated greater conformational flexibility in the terminal residues and loop region but minor fluctuations in the core structural and binding site residues, indicating stable interactions of the protein–ligand complex. The stable radius of gyration (~ 1.54–1.57 nm) suggests stable protein compactness upon ligand binding (Fig. 6D). Additionally, the protein—ligand interaction energy values (Fig. 6E) remained steadily favorable throughout the 100 ns simulation, highlighting stable noncovalent binding.

4. Discussion

Toxic hepatitis, or drug-induced liver injury, is a multifactorial liver injury that involves complex pathological processes driven by oxidative stress, inflammatory responses and dysregulated hepatocellular pathways, leading to several therapeutic complications. Owing to limited conventional treatment options, plant-based interventions that exhibit multitarget therapeutic capabilities are increasingly promising alternatives. The present study employed an integrated computational framework to study the role of moringa oleifera seed extract as a hepatoprotective agent in the treatment of toxic hepatitis via high-resolution mass spectrometry (HRMS)-driven constituent identification, ADMET profiling, similarity ensemble approach (SEA)-based target prediction, protein–protein interaction (PPI) network construction with Mathiew correlation coefficient (MCC) hub identification, Metascape enrichment, SMINA molecular docking, and 100 ns molecular dynamic (MD) simulation. This multilayered approach with computational systems pharmacology provides unprecedented mechanistic depth for traditional remedies.

HRMS profiling, conducted on a Q-TOF system with electrospray ionization, accurate mass errors (< 5 ppm) and diagnostic MS/MS fragments, yielded high-fidelity annotations of 3085 phytochemicals of diverse classes, such as polyphenols, isothiocyanates, flavonoids, phenolic acids and alkaloids, in the MOSE extract, highlighting the correlation with literature-documented hepatoprotection via antioxidant, anti-inflammatory, and detoxifying properties. This metabolome served as the scaffold for downstream analysis. After subsequent filtering on the basis of abundance thresholds, ADMET analysis via SwissADME, Protox II and pkCSM filtered out phytocompounds, prioritizing those with optimal Lipinski/Veber compliance (0 violations), high gastrointestinal absorption (> 70%), low hepatotoxicity risks, AMES negativity, and CYP3A4/CYP2D6 inhibition liabilities, which are crucial for hepatoprotective intervention. Pains and brenk alerts were also considered to avoid false bioactive positivity. However, trans-3-indoleacrylic acid was retained even after a single Michael acceptor alert, as no Brenk structural toxicity alert was present, and all other ADME parameters were favorable. Hence, trans-3-indoleacrylic acid, 5-(4-morpholinyl)pyrazolo[1,5-a]quinazoline-3-carbonitrile and R-prunasin were identified as lead bioactive compounds with highly satisfactory absorption and toxicity after ADMET screening.

Prediction of the targets of these compounds through the similarity ensemble approach and their intersection with toxic hepatitis-related genes obtained from DisGeNET and GeneCards through Venny predicted 13 targets with good similarity. Network pharmacology involves the construction of a comprehensive compound–target–disease interactome and the mapping of HRMS hits to validated hepatotoxicity pathways. Five hub genes were identified with the help of Cytoscape: HRAS, PIK3CA, LGALS3, MMP9 and NFE2L2, which represent key biological processes involved in DILI.

Previous studies revealed that nuclear factor erythroid 2-related factor 2 (NFE2L2 or NFR2) is the predominant regulator of oxidative stress and inflammation-related disorders. Under normal conditions, it remains associated with its main inhibitor Kelch-like ECH-associated protein 1 (Keap 1) in the cytosol, but under oxidative stress, it separates from Keap1 and activates key antioxidant enzymes such as superoxide dismutase (SOD), glutathione-S-transferase (GST), heme oxygenase-1 (HO-1) and catalase (CAT), which are responsible for converting harmful reactive oxygen species such as H_2O_2 into harmless water and oxygen, thus preventing the oxidative stress produced during drug metabolism (34, 35). In addition, NFE2L2 also downregulates the activation of the signaling protein c-Jun N-terminal kinase (JNK) (36) and upregulates the expression of the Bcl-2 protein necessary to inhibit the release of cytochrome C in mitochondria, which prevents cell death or apoptosis in the context of toxic hepatitis (37). In this context, trans-3-indoleacrylic acid may act as an indirect supporter of NFE2L2-mediated antioxidant mechanisms, in line with the literature describing indole-derived compounds as regulators of NF-κB-driven inflammatory and cellular redox equilibrium pathways rather than direct enzyme targeting. HRAS and PIK3CA are the major influencers of the MAPK/ERK and AKT/PI3K pathways involved in hepatocarcinogenesis (38) and propagate receptor tyrosine kinase (RTK)-driven autophosphorylation, leading to apoptosis resistance and increased tumor cell survival (39, 40). Along with MMP9, they are known to interact with nuclear receptors such as PPARs or AhR to regulate the transcription of anti-inflammatory genes and maintain cellular homeostasis by activating stress-activated cascades (41, 42). Matrix metalloproteinase-9 (MMP9) and LGALS3 are primarily involved in NF-κB-driven inflammatory responses and extracellular matrix (ECM) remodeling and play vital roles in liver regeneration (42–44). Our network pharmacology results perfectly align with these established mechanisms of hub targets. NFE2L2 is strongly associated with pathways related to apoptotic regulation (positive and negative), reactive oxygen species signaling and nuclear receptor signaling, indicating its potential involvement in antioxidant and cytoprotective mechanisms. HRAS and PIK3CA were mapped to pathways associated with receptor tyrosine kinase-activated signaling, nuclear receptor signaling, the cellular response to environmental and abiotic stimuli, the response to peptide hormones and chemical carcinogenesis. These findings suggest their role in RTK-mediated survival signaling and antioxidant mechanisms. Additionally, MMP9 was found to be involved in the cellular response to environmental stimuli, the cellular response to abiotic stimuli, chemical carcinogenesis-ROS, the regulation of the apoptotic signaling pathway and signaling by receptor tyrosine kinases, whereas LGALS3 was found to be responsible for the positive and negative regulation of apoptotic pathways. These findings indicate the significant collaboration of these hub targets with multiple pathways relevant to inflammation, oxidative stress regulation and cell viability.

This multi-target relationship with the hub genes was further corroborated by molecular docking and 100 ns simulation to provide structural validation of network pharmacology predictions. The docking results revealed that all three shortlisted

compounds consistently strongly interact with the five hub genes with notably stronger affinity observed for R-Prunasin with HRAS (-9.20 kcal/mol), followed by R-Prunasin with PIK3CA (-7.90 k kcal/mol), indicating that despite being a cyanogenic agent, its specific functional groups allow it to form stable complexes, ensuring cellular homeostasis and uninterrupted survival signaling toward the nucleus, even under adverse conditions. Since both HRAS and PIK3CA mediate RTK signaling, it also reflects that cyanogenic glycosides may exert phytochemical-influenced biological activity rather than acting as sole toxic agents. Their stability with R-Prunasin also suggests that R-Prunasin may lower the cutoff required for the liver to initiate regeneration after being affected by toxins. This is further validated by the excellent convergence obtained during a 100 ns simulation of the R-Prunasin-HRAS complex. Rapid convergence of protein and ligand RMSD values and a stable radius of gyration provided strong evidence that the complex reached an early equilibrium state, which does not undergo any unnatural structural distortions under simulated physiological conditions, which is essential for its survival signaling role in combatting toxic hepatitis. The RMSF values, which are indicative of amino acid flexibility, also fluctuated slightly, confirming that R-Prunasin binds with HRAS tightly and prevents other harmful metabolites from hindering HRAS signaling. Another robust docking finding between 5-(4-morpholinyl)pyrazolo[1,5-a]quinazoline-3-carbonitrile and PIK3CA (-7.77 ± 0.06 kcal/mol) suggested that by targeting the active site of PIK3CA through competitive inhibition, this morpho-compound likely modulates PI3K/AKT mechanisms, which are often dysregulated during inflammatory toxic stress. This potentially limits the secondary wave of liver damage following excessive immune activation due to primary toxin exposure. Collectively, the integrated systems-level computational framework of HRMS extraction, ADMET screening, and a network pharmacology approach validated by molecular docking and simulation analyses suggest that the hepatoprotective effect of MOSE extract may arise from synergy between multiple compounds that modulate multiple oxidative, inflammatory and apoptotic pathways implicated in toxic hepatitis, suggesting that future experimental validation should be carried out to authenticate in silico predictions.

Declarations

Conflicts of interest:

The authors have no conflicts of interest to declare that are relevant to the content of this article.

Funding:

No funding was received for conducting this study.

Author Contribution

N.G. drafted the manuscriptR.M. supervised and guided the research activities J.S. supervised and guided the research activities B.P. performed ADMET analysisA.A. data collectionA.T. final manuscript preparation

References

1. Devarbhavi H, Joseph T, Kumar NS, Rathi C, Thomas V, Singh SP et al (2021) The Indian network of drug-induced liver injury: etiology, clinical features, outcome and prognostic markers in 1288 patients. J Clin Exp Hepatol 11(3):288–298
2. Shen T, Liu Y, Shang J, Xie Q, Li J, Yan M et al (2019) Incidence and etiology of drug-induced liver injury in mainland China. Gastroenterology 156(8):2230–2241
3. Andrade RJ, Chalasani N, Björnsson ES, Suzuki A, Kullak-Ublick GA, Watkins PB et al (2019) Drug-induced liver injury. Nat Rev Dis Prim 5(1):58
4. Leise MD, Poterucha JJ, Talwalkar JA (2014) Drug-induced liver injury. In: Mayo clinic proceedings. Elsevier; pp. 95–106
5. Stehbens WE (2003) Oxidative stress, toxic hepatitis, and antioxidants with particular emphasis on zinc. Exp Mol Pathol 75(3):265–276

6. Weaver RJ, Betts C, Blomme EAG, Gerets HHJ, Gjervig Jensen K, Hewitt PG et al (2017) Test systems in drug discovery for hazard identification and risk assessment of human drug-induced liver injury: Industry-led perspective from EFPIA members of the EU Innovative Medicines Initiative Drug Liver Injury Project, MIP Dili. Expert Opin Drug Metab Toxicol 13(7):767–782
7. Cao X, Shi K, Xu Y, Zhang P, Zhang H, Pan S (2023) Integrated metabolomics and network pharmacology to reveal antioxidant mechanisms and potential pharmacological ingredients of citrus herbs. Food Res Int 174:113514
8. Karthikkeyan G, Pervaje R, Subbannayya Y, Patil AH, Modi PK, Prasad TSK (2020) Plant omics: metabolomics and network pharmacology of liquorice. Indian Ayurvedic Med Yashtimadhu Omi J Integr Biol 24(12):743–755
9. Ibrahim RE, El-Houseiny W, Behairy A, Mansour MF, Abd-Elhakim YM (2019) Ameliorative effects of Moringa oleifera seeds and leaves on chlorpyrifos-induced growth retardation, immune suppression, oxidative stress, and DNA damage in Oreochromis niloticus. Aquaculture 505:225–234
10. Dzuvor CKO, Pan S, Amanze C, Amuzu P, Asakiya C, Kubi F (2022) Bioactive components from Moringa oleifera seeds: production, functionalities and applications–a critical review. Crit Rev Biotechnol 42(2):271–293
11. Gopalakrishnan L, Doriya K, Kumar DS (2016) Moringa oleifera: A review on nutritive importance and its medicinal application. Food Sci Hum wellness 5(2):49–56
12. Orfali R, Perveen S, Siddiqui NA, Alam P, Alhowiriny TA, Al-Taweel AM et al (2019) Pharmacological evaluation of secondary metabolites and their simultaneous determination in the Arabian medicinal plant Plicosepalus curviflorus using HPTLC validated method. J Anal Methods Chem 2019(1):7435909
13. Banerjee S, Bhattacharjee P, Kar A, Mukherjee PK (2019) LC–MS/MS analysis and network pharmacology of Trigonella foenum-graecum–A plant from Ayurveda against hyperlipidemia and hyperglycemia with combination synergy. Phytomedicine 60:152944
14. Sharma B, Yadav DK (2022) Metabolomics and network pharmacology in the exploration of the multi-targeted therapeutic approach of traditional medicinal plants. Plants 11(23):3243
15. Singh A, Tandon S, Nandi SP, Kaur T, Tandon C (2021) Downregulation of inflammatory mediators by ethanolic extract of Bergenia ligulata (Wall.) in oxalate injured renal epithelial cells. J Ethnopharmacol 275:114104
16. Matulyte I, Marksa M, Ivanauskas L, Kalvėnienė Z, Lazauskas R, Bernatoniene J (2019) GC–MS analysis of the composition of the extracts and essential oil from Myristica fragrans seeds using magnesium aluminometasilicate as excipient. Molecules 24(6):1062
17. Bi Y, Han X, Lai Y, Fu Y, Li K, Zhang W et al (2021) Systems pharmacological study based on UHPLC-Q-Orbitrap-HRMS, network pharmacology and experimental validation to explore the potential mechanisms of Danggui-Shaoyao-San against atherosclerosis. J Ethnopharmacol 278:114278
18. Mukherjee PK, Banerjee S, Kar A (2021) Molecular combination networks in medicinal plants: understanding synergy by network pharmacology in Indian traditional medicine. Phytochem Rev 20(4):693–703
19. Daina A, Michielin O, Zoete V (2017) SwissADME: a free web tool to evaluate pharmacokinetics, drug-likeness and medicinal chemistry friendliness of small molecules. Sci Rep 7:42717
20. Banerjee P, Kemmler E, Dunkel M, Preissner R (2024) ProTox 3.0: a webserver for the prediction of toxicity of chemicals. Nucleic Acids Res 52(W1):W513–W520
21. Pires DEV, Blundell TL, Ascher DB (2015) pkCSM: predicting small-molecule pharmacokinetic and toxicity properties using graph-based signatures. J Med Chem 58(9):4066–4072
22. Keiser MJ, Roth BL, Armbruster BN, Ernsberger P, Irwin JJ, Shoichet BK (2007) Relating protein pharmacology by ligand chemistry. Nat Biotechnol 25(2):197–206
23. Stelzer G, Rosen N, Plaschkes I, Zimmerman S, Twik M, Fishilevich S et al (2016) The GeneCards suite: from gene data mining to disease genome sequence analyses. Curr Protoc Bioinforma 54(1):1–30
24. Piñero J, Ramírez-Anguita JM, Saüch-Pitarch J, Ronzano F, Centeno E, Sanz F et al (2020) The DisGeNET knowledge platform for disease genomics: 2019 update. Nucleic Acids Res 48(D1):D845–D855

25. Oliveros JC (2007) VENNY. An interactive tool for comparing lists with Venn Diagrams. http//bioinfogp cnb csic es/tools/venny/index html
26. Szklarczyk D, Kirsch R, Koutrouli M, Nastou K, Mehryary F, Hachilif R et al (2023) The STRING database in 2023: protein–protein association networks and functional enrichment analyses for any sequenced genome of interest. Nucleic Acids Res 51(D1):D638–D646
27. Shannon P, Markiel A, Ozier O, Baliga NS, Wang JT, Ramage D et al (2003) Cytoscape: a software environment for integrated models of biomolecular interaction networks. Genome Res 13(11):2498–2504
28. Zhou Y, Zhou B, Pache L, Chang M, Khodabakhshi AH, Tanaseichuk O et al (2019) Metascape provides a biologist-oriented resource for the analysis of systems-level datasets. Nat Commun 10(1):1523
29. Berman HM, Westbrook J, Feng Z, Gilliland G, Bhat TN, Weissig H et al (2000) The protein data bank. Nucleic Acids Res 28(1):235–242
30. Koes DR, Baumgartner MP, Camacho CJ (2013) Lessons learned in empirical scoring with smina from the CSAR 2011 benchmarking exercise. J Chem Inf Model 53(8):1893–1904
31. Abraham MJ, Murtola T, Schulz R, Páll S, Smith JC, Hess B et al (2015) GROMACS: High performance molecular simulations through multi-level parallelism from laptops to supercomputers. SoftwareX 1:19–25
32. Darden T, York D, Pedersen L (1993) Particle mesh Ewald: An N log (N) method for Ewald sums in large systems. J Chem Phys 98:10089
33. Páll S, Hess B (2013) A flexible algorithm for calculating pair interactions on SIMD architectures. Comput Phys Commun 184(12):2641–2650
34. Xu Q, Fan Y, Loor JJ, Liang Y, Sun X, Jia H et al (2020) Cardamonin reduces acetaminophen-induced acute liver injury in mice autophagy and NFE2L2 signaling. Front Pharmacol 11:601716
35. Aborehab NM, Waly NE (2019) IL-6 and NFE2L2: A putative role for the hepatoprotective effect of N. Sativa, P. Ginseng and C. Sempervirens in AFB-1 induced hepatocellular carcinoma in rats. Toxicol Rep 6:457–464
36. Li J, Tian M, Hua T, Wang H, Yang M, Li W et al (2021) Combination of autophagy and NFE2L2/NRF2 activation as a treatment approach for neuropathic pain. Autophagy 17(12):4062–4082
37. Pajares M, Jiménez-Moreno N, García-Yagüe ÁJ, Escoll M, de Ceballos ML, Van Leuven F et al (2016) Transcription factor NFE2L2/NRF2 is a regulator of macroautophagy genes. Autophagy 12(10):1902–1916
38. Fang X, Cai Y, Zhao Z, Yang S, Li Z, Peng X et al (2025) Mechanisms of HRAS regulation of liver hepatocellular carcinoma for prognosis prediction. BMC Cancer 25(1):1–16
39. Santra T, Herrero A, Rodriguez J, von Kriegsheim A, Iglesias-Martinez LF, Schwarzl T et al (2019) An integrated global analysis of compartmentalized HRAS signaling. Cell Rep 26(11):3100–3115
40. Liu Z, Hou P, Ji M, Guan H, Studeman K, Jensen K et al (2008) Highly prevalent genetic alterations in receptor tyrosine kinases and phosphatidylinositol 3-kinase/akt and mitogen-activated protein kinase pathways in anaplastic and follicular thyroid cancers. J Clin Endocrinol Metab 93(8):3106–3116
41. Casado P, Bilanges B, Rajeeve V, Vanhaesebroeck B, Cutillas PR (2014) Environmental stress affects the activity of metabolic and growth factor signaling networks and induces autophagy markers in MCF7 breast cancer cells. Mol Cell Proteom 13(3):836–848
42. Naim A, Pan Q, Baig MS (2017) Matrix metalloproteinases (MMPs) in liver diseases. J Clin Exp Hepatol 7(4):367–372
43. Lurje I, Biegel DK, Zhang IW, Tacke F (2026) The Role of Galectin-3 in Liver Inflammation and Fibrosis. J Inflamm Res. ;1–21
44. Pang T, Fu J, Li J, Chen Y, He H, Ma J et al (2024) Screening of common key immune genes and prediction of potential drugs in chronic hepatic injury

Table 1

Table 1 is available in the Supplementary Files section.

Figures

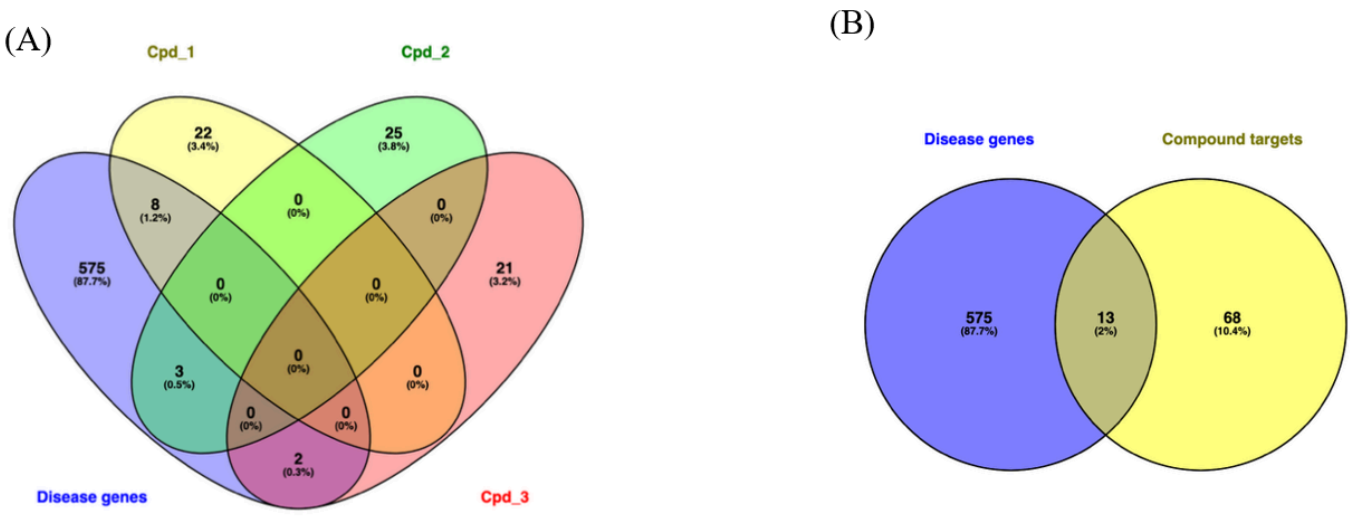

Figure 1

(A). Venn diagram intersection of toxic hepatitis associated genes with each compound target. Cpd_1= trans-3-indoleacrylic acid, Cpd_2=(R)-Prunasin, Cpd_3= 5-(4-Morpholinyl)pyrazol[1,5a]quinazoline-3-carbonitrile. (B) Venn diagram intersection of all three compound targets and toxic hepatitis targets

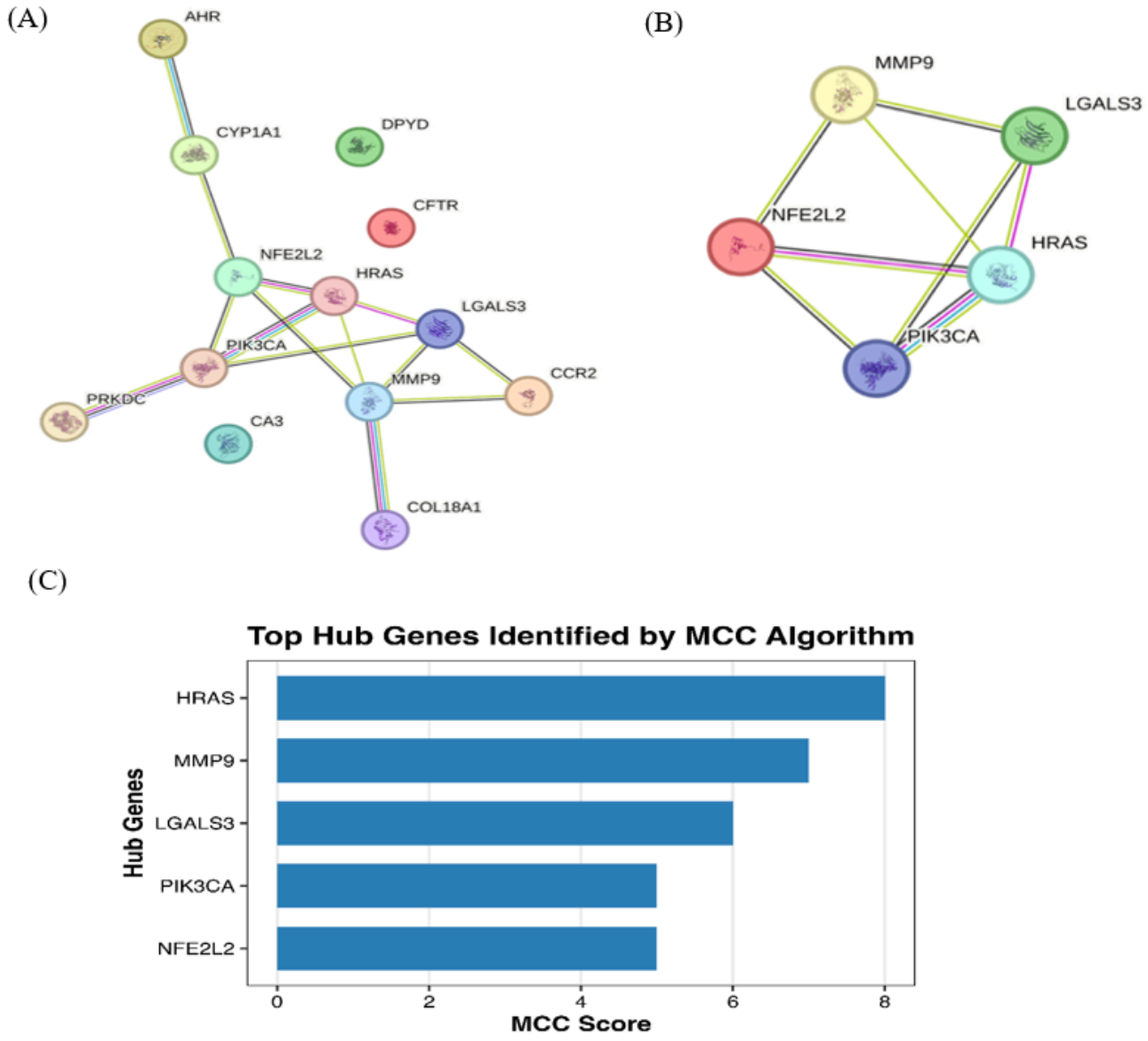

Figure 2

(A) String PPI network of all disease-associated genes of compounds. (B) String PPI network of the top 5 hub genes associated with toxic hepatitis through CytoNCA. (C) Top hub genes ranked by the MCC algorithm in cytohubba.

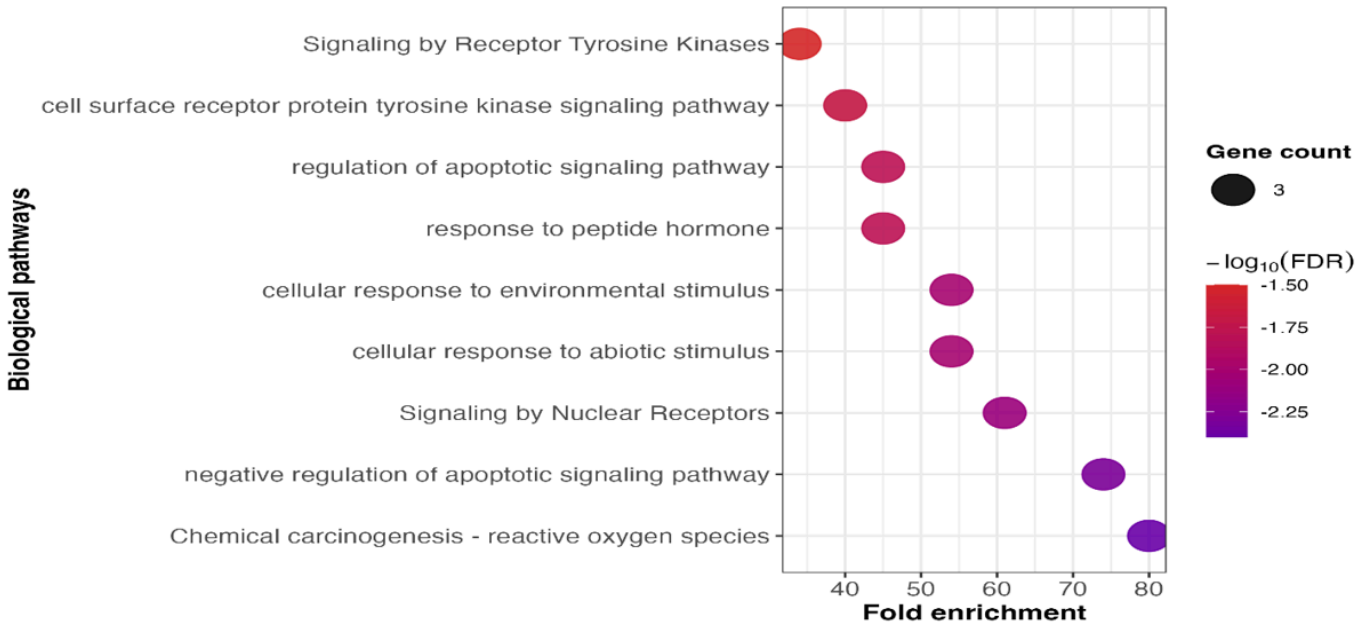

Figure 3

Biological pathway enrichment dot plot for toxic hepatitis related genes. X-axis represent fold enrichment and Y- axis denotes pathways. Dot size corresponds to gene count and color gradient shows the statistical significance level ($-\log_{10}$(q-value).

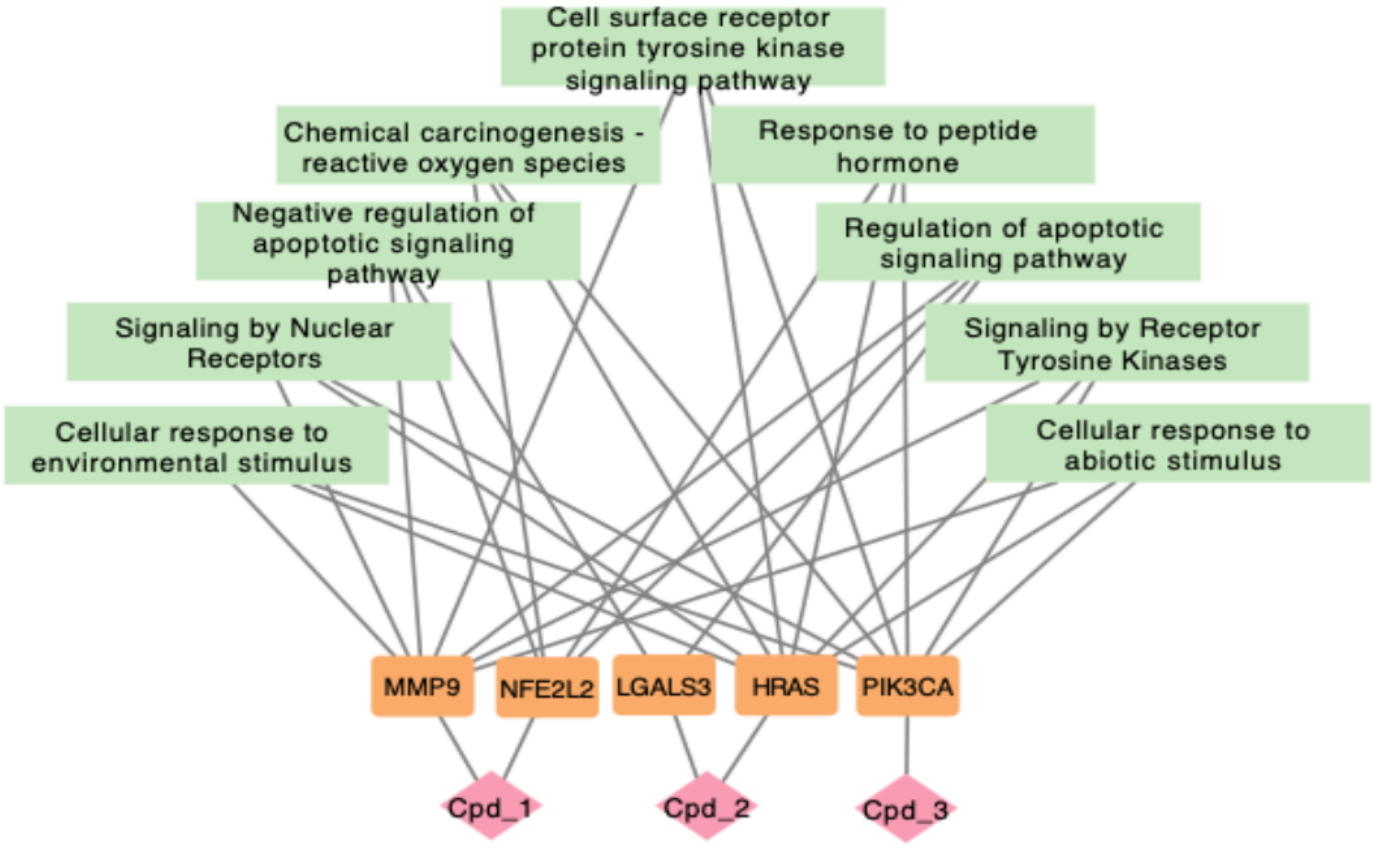

Figure 4

Compound-target-pathway network generated by Cytoscape. Diamond represents compounds trans-3-indoleacrylic acid (Cpd_1), (R)-Prunasin (Cpd_2) and 5-(4-Morpholinyl)pyrazolo[1,5-a]quinazoline-3-carbonitrile (Cpd_3), rounded rectangles denote gene targets and rectangles indicate pathways mediated by the genes.

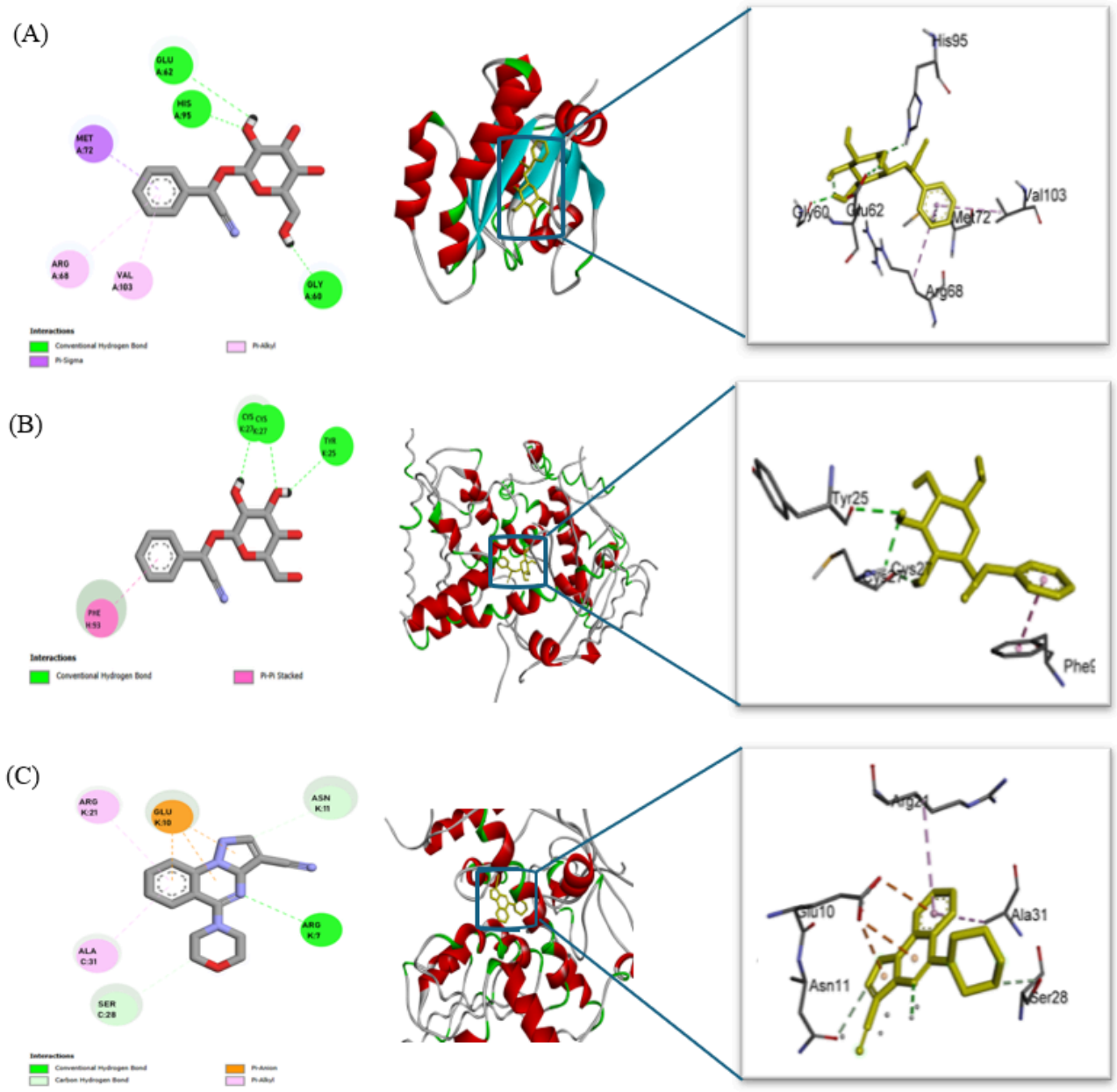

Figure 5

2D and 3D interaction of complexes (A) R-Prunasin with HRAS (PDB ID 9IAY). (B) R-Prunasin with PIK3CA (8EXL). (C) 5-(4-Morpholinyl)pyrazolo[1,5-a]quinazoline-3-carbonitrile with PIK3CA (8EXL).

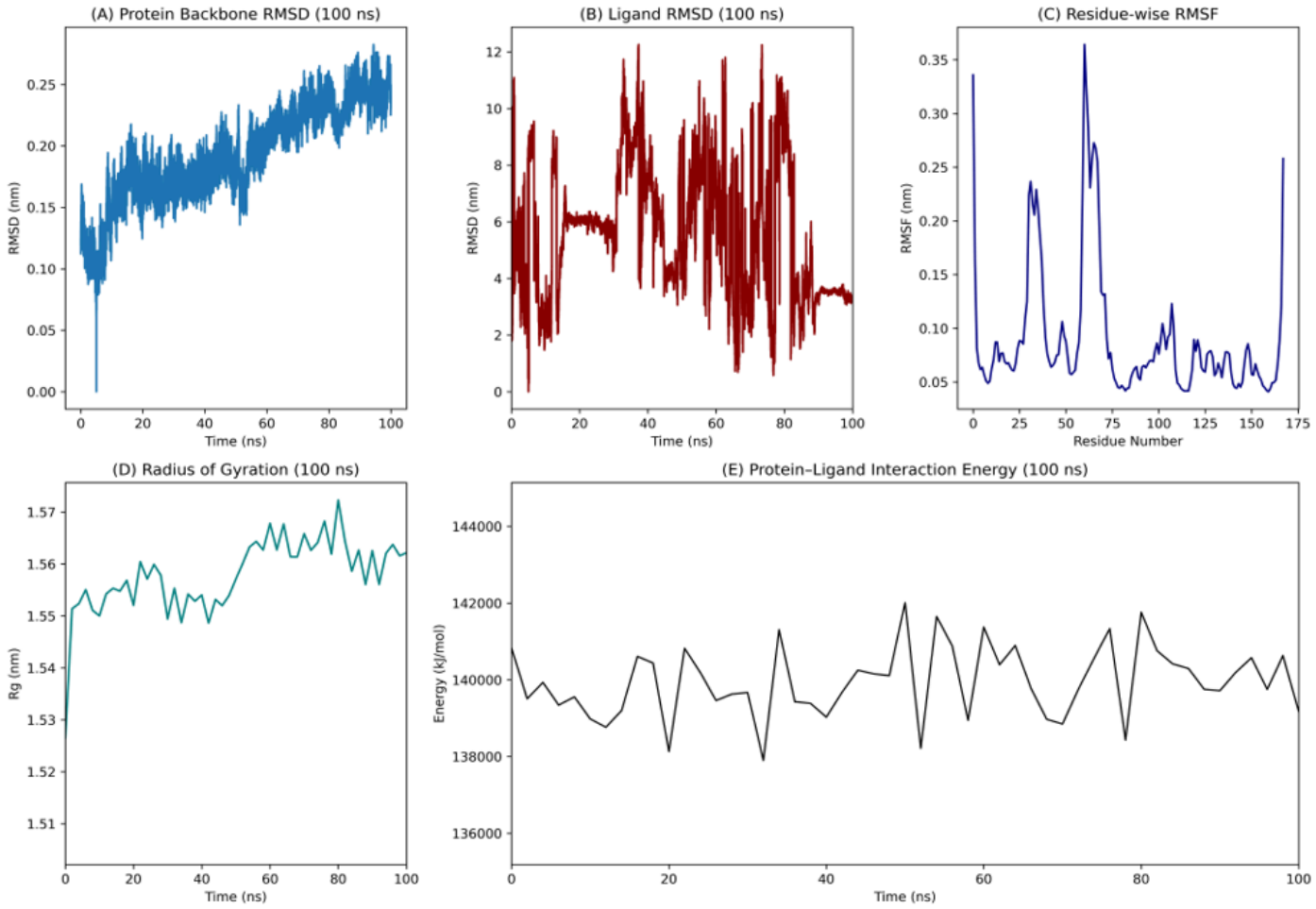

Figure 6

Molecular Dynamics Simulation analysis of (R)-Prunasin-HRAS docked complex over 100ns trajectory. (A) Protein HRAS backbone root mean square deviation (RMSD) as a function of time. (B) Ligand RMSD profile as a function of time. (C) Residue wise root mean square fluctuation (RMSF) of HRAS upon ligand binding as a function of time. (D) Radius of Gyration (Rg) plot as a function of time. (E)Protein- ligand interaction energy plot as a function of time.

Supplementary Files

This is a list of supplementary files associated with this preprint. Click to download.

- Supplementaryfiles.docx
- Table1.docx
- GA.png